

## Programmable atom-photon quantum interface

Christoph Kurz, Pascal Eich, Michael Schug, Philipp Müller, and Jürgen Eschner<sup>\*</sup>  
*Universität des Saarlandes, Experimentalphysik, Campus E2 6, 66123 Saarbrücken, Germany*

(Received 22 March 2016; published 30 June 2016)

We present the implementation of a programmable atom-photon quantum interface, employing a single trapped  $^{40}\text{Ca}^+$  ion and single photons. Depending on its mode of operation, the interface serves as a bidirectional atom-photon quantum-state converter, as a source of entangled atom-photon states, or as a quantum frequency converter of single photons. The interface lends itself particularly to interfacing ions with spontaneous parametric down-conversion-based single-photon or entangled-photon-pair sources.

DOI: [10.1103/PhysRevA.93.062348](https://doi.org/10.1103/PhysRevA.93.062348)

### I. INTRODUCTION

Quantum networks [1] integrate quantum-information processing and storage devices with quantum communication channels, allowing one to distribute quantum information between stationary network nodes through flying quantum bits (qubits). A platform that has proven suitable for this purpose is the combination of single trapped ions and single photons: while single ions allow for storing and processing quantum information [2–4], single photons are the only viable carriers of quantum information over long distances [5,6]. To interconvert stationary and flying qubits, quantum interfaces are needed. Different approaches for the experimental implementation of atom-photon quantum interfaces have emerged. These include objectives and lenses of high numerical aperture [7,8], deep parabolic mirrors [9,10], and optical resonators [11–14]. With these systems, a number of essential quantum-networking building blocks have been realized, such as atom-photon entanglement [15,16], atom-to-photon quantum-state mapping [17–19], heralded atom-atom entanglement [20,21], quantum teleportation [22], and direct quantum-state transfer [23]. We demonstrated further basic prerequisites of a quantum network such as the high-rate generation of single photons in a pure quantum state [24] and the direct photonic interaction between distant single ions [25]. Recently, we implemented a protocol for high-fidelity heralded transfer of a photonic polarization qubit onto the qubit state of a single ion [26].

Here we report on a significant and comprehensive extension of that protocol, the realization of a programmable, bidirectional interface between a single ion and single photons, which depending on its mode of operation permits atom-to-photon or photon-to-atom quantum-state transfer, as well as generation of atom-photon entanglement; moreover, it is also suitable for quantum frequency conversion of single photons. Thereby the interface covers the essential operations required in quantum networks and especially for a quantum repeater [27].

### II. INTERFACE PRINCIPLE

Figure 1 illustrates the general principle of the interface, experimentally implemented with the ground and excited states of a single  $^{40}\text{Ca}^+$  ion. We first create a coherent

superposition of the two outer Zeeman sublevels of the metastable  $D_{5/2}$  state,

$$|\psi_D\rangle = \cos\frac{\vartheta_D}{2}|D, -\frac{5}{2}\rangle + \sin\frac{\vartheta_D}{2}e^{i\varphi_D}|D, +\frac{5}{2}\rangle, \quad (1)$$

and expose the ion to resonant photons on the  $D_{5/2}$  to  $P_{3/2}$  transition at 854 nm which are in a polarization state in the circular basis,

$$|\psi_{854}\rangle = \cos\frac{\vartheta_{854}}{2}|854, R\rangle + \sin\frac{\vartheta_{854}}{2}e^{i\varphi_{854}}|854, L\rangle, \quad (2)$$

such that the input state of the interface is  $|\Psi_{\text{in}}\rangle = |\psi_D\rangle|\psi_{854}\rangle$ . Right-handed ( $R$ ) and left-handed ( $L$ ) circularly polarized 854-nm photons may be absorbed on the  $\sigma^+$  and  $\sigma^-$  transition, respectively. Absorption of a photon triggers the emission of a single Raman photon on the  $P_{3/2}$  to  $S_{1/2}$  transition at 393 nm and transfers the ion to the  $S_{1/2}$  ground state. For detection along the quantization axis, the two possible transitions,  $\sigma^+$  and  $\sigma^-$ , translate to  $R$ - and  $L$ -polarized 393-nm photons, respectively. We hence obtain the ion-photon output state

$$|\Psi_{\text{out}}\rangle = \cos\frac{\theta}{2}|S, -\frac{1}{2}\rangle|393, L\rangle + \sin\frac{\theta}{2}e^{i\phi}|S, +\frac{1}{2}\rangle|393, R\rangle. \quad (3)$$

The evolution of the system from  $|\Psi_{\text{in}}\rangle$  into the entangled state  $|\Psi_{\text{out}}\rangle$  is described by [28]

$$|\Psi_{\text{out}}\rangle = (|S, -\frac{1}{2}\rangle|393, L\rangle\langle D, -\frac{5}{2}|854, R| + |S, +\frac{1}{2}\rangle|393, R\rangle\langle D, +\frac{5}{2}|854, L|) \cdot |\Psi_{\text{in}}\rangle$$

and used to realize the different interface operations: (i) when  $|\psi_D\rangle$  and  $|\psi_{854}\rangle$  are fixed, entangled atom-photon pairs are created (entangler operation); (ii) when  $|\Psi_{\text{out}}\rangle$  is projected by detecting the 393-nm photon in a linear basis, the polarization state of the absorbed 854-nm photon is mapped into an atomic qubit state in  $S_{1/2}$  (receiver operation); (iii) when the final atomic state is projected on a superposition of the Zeeman sublevels, the initial atomic state  $|\psi_D\rangle$  is mapped into the polarization qubit of the output 393-nm photon (sender operation); (iv) finally, when both atomic superpositions are fixed, any input photon will be converted into a frequency-converted output photon of the corresponding polarization (converter operation). Receiver operation has been shown in [26], entangler and sender operation are demonstrated below. Quantum frequency conversion of photons from 854 to 393 nm is implicitly realized by these demonstrations.

<sup>\*</sup>juergen.eschner@physik.uni-saarland.de



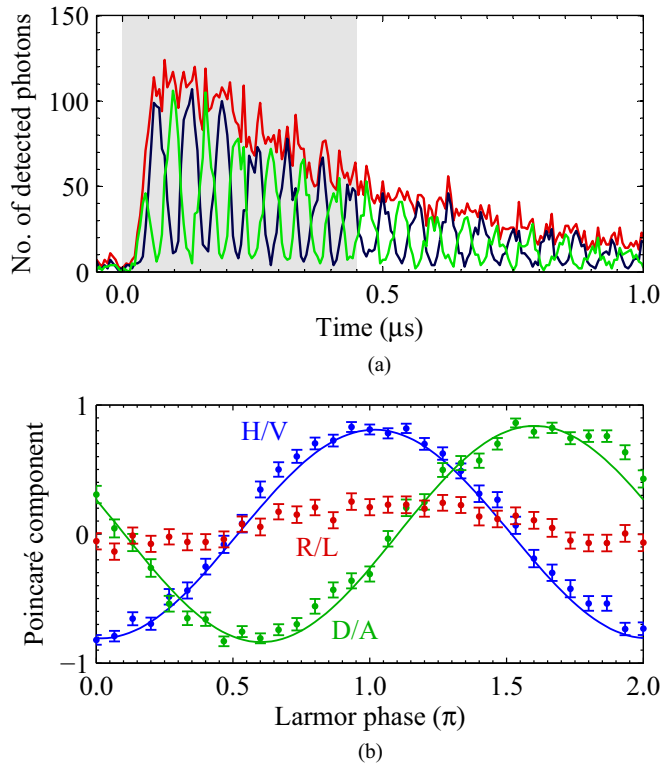


FIG. 3. Polarization analysis of single 393-nm photons. (a) Conditional photon arrival-time histograms, shown for photons projected onto the horizontal (blue or dark gray line) and vertical (green or light gray line) polarization states, and conditioned on the projection of the ion onto the state  $|+\rangle$ . The red (medium gray) curve shows the unconditioned arrival-time distribution, i.e., the sum of the blue and green histograms. The shaded area represents the time window used for data analysis. The bin size is 5 ns and the overall measuring time is 20 min. (b) State tomography of the photonic polarization for the same atomic-state preparation and projection as in (a). Shown are the three Poincaré components as functions of the Larmor phase. The solid lines are sinusoidal fits.

#### IV. ENTANGLER OPERATION

To verify the operation of our interface as a source of entangled ion-photon states, we perform standard quantum-state tomography [32] of the two-qubit system through correlation measurements in the product bases of photonic and atomic qubits. Using a maximum-likelihood approach [32], we reconstruct the physical quantum state that is most likely to have produced the experimental data. From the derived density matrix, depicted in Fig. 4, we find a fidelity  $F = 84.6(2)\%$  with respect to the maximally entangled state [Eq. (3)] for our 450-ns time window. This value exceeds the classical threshold of  $\frac{2}{3}$  by more than 80 standard deviations and thus clearly indicates the creation of entanglement at the output of our interface.

The two main sources of infidelity in our setup are currently the magnetic-field fluctuations which limit the atomic coherence time and, as mentioned above, the imperfectly calibrated wave plates. The photon-detection efficiency for this experiment amounts to 0.353(1)%, including that only 50% of the arriving photons are transmitted through the

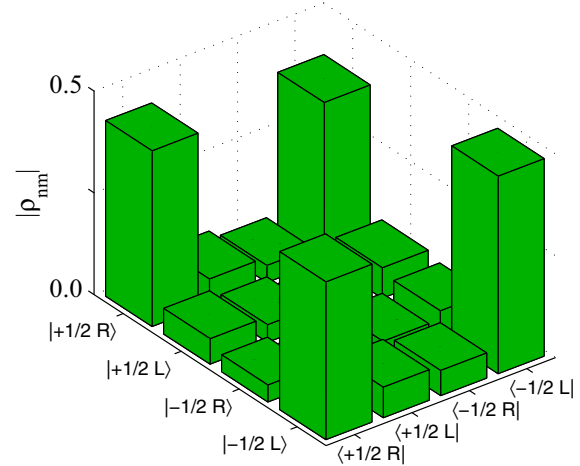


FIG. 4. Density matrix of the entangled ion-photon state in the product basis. Shown are the moduli of the matrix entries.

polarization analyzer. At 11-kHz repetition rate and taking the PMT quantum efficiency of 28(1)% into account, we obtain  $140(5)\text{ s}^{-1}$  fiber-coupled photons that are entangled with the ion; removing the polarization analysis would double that rate.

#### V. SENDER OPERATION

Operation of our interface for ion-to-photon quantum-state transfer is accomplished when a prepared atomic input state, characterized by angles  $\vartheta_D$  and  $\varphi_D$  [Eq. (1)], leads to the emission of a 393-nm output photon in the corresponding polarization state. This interface operation involves projection of the final atomic state onto a fixed superposition, for which we choose the  $|+\rangle$  state. In this case the 393-nm photon detected at time  $t$  will be described by

$$|\psi_{393}\rangle = \cos\frac{\theta}{2}|R\rangle - \sin\frac{\theta}{2}e^{i\phi}|L\rangle, \quad (5)$$

with  $\theta = \vartheta_D$  and  $\phi = \varphi_{729} + \omega_L t$ . One sees that the Larmor precession of the input state enters into the polarization of the output state. This is convenient for verification of the interface (see below); it has to be taken into account as a time-dependent phase shift when the interface is operated in a quantum communication scenario.

First, we prepare the four symmetric ( $\vartheta_D = \frac{\pi}{2}$ ) superposition states with  $\varphi_{729} = \{0, \frac{\pi}{2}, \pi, \frac{3\pi}{2}\}$  and analyze the photonic phase, i.e., the direction of the linear polarization of the 393-nm photon. The result is displayed in Fig. 5(a): the linear dependence with steps of  $\frac{\pi}{2}$  between the four lines shows that the photonic phase reflects faithfully both the Larmor phase  $\omega_L t$  and  $\varphi_{729}$ .

In a second step, we perform full quantum-process tomography of the atom-to-photon state mapping process by using also the bare input states  $|\pm\frac{\pi}{2}\rangle$  and analyzing the photonic state in all three polarization bases. This allows us to reconstruct the process matrix  $\chi$ , defined through  $\rho_{\text{out}} = \sum_{m,n} \chi_{mn} \sigma_m \rho_{\text{in}} \sigma_n$  with the Pauli matrices  $\{\sigma_{i=1,\dots,4}\} = \{\mathbb{1}, \sigma_x, \sigma_y, \sigma_z\}$  [33]. The matrix is displayed in Fig. 5(b). The value  $\chi_{11}$  represents the identity part of the quantum process and is known as the process fidelity. From our experimental data, we derive

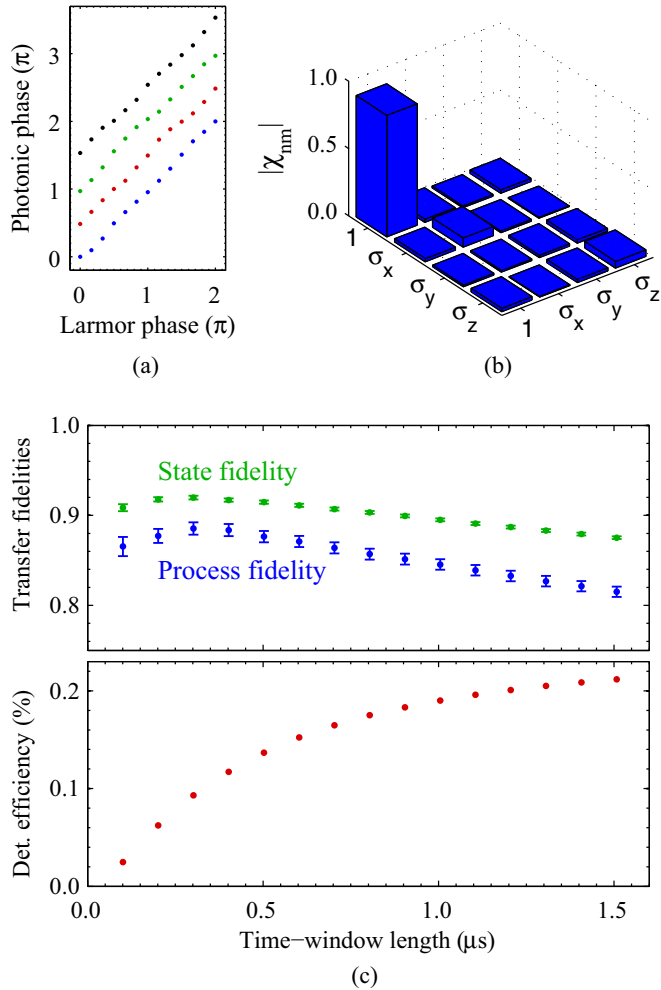


FIG. 5. Characterization of ion-to-photon quantum-state transfer. (a) Phase of the photon’s linear polarization as a function of the Larmor phase and for  $\varphi_{729} = \{0, \frac{\pi}{2}, \pi, \frac{3\pi}{2}\}$  (top to bottom). (b) Quantum-process matrix in the Pauli basis. Shown are the moduli of the matrix entries. (c) Process fidelity (blue dots), mean quantum-state fidelity (green dots), and detection efficiency for different lengths of the detection time window. Where not indicated, error bars are smaller than the size of the symbols.

$\chi_{11} = 90.2(1.0)\%$ . Another measure for the quality of the state transfer is the mean fidelity of the reconstructed photonic states with respect to the atomic input states; averaged over all six input states, it amounts to  $92.4(3)\%$ . It is instructive to investigate how the two figures of merit behave as a function of the detection time window, which is depicted in Fig. 5(c); the same figure shows the tradeoff between fidelity and success

probability of the interface. For the 450-ns time window, we achieve  $0.127(1)\%$  mean photon detection efficiency. At a 10-kHz repetition rate, we obtain  $45(2) \text{ s}^{-1}$  fiber-coupled photons. The efficiency reduction compared to the previous measurement is caused by using different wave plates that are better calibrated but have smaller apertures. Removing the wave plates and polarizer would allow us to transfer the atomic qubit state onto fiber-coupled photons at an estimated rate of  $\sim 300 \text{ s}^{-1}$ , similar to that for ion-photon entanglement.

An important source of infidelity for both ion-photon entanglement and ion-to-photon quantum-state transfer are magnetic-field fluctuations in the vicinity of the trap apparatus that limit the coherence of the atomic qubit state. We expect to mitigate this issue by means of an active magnetic-field stabilization. Additional minor sources of infidelity are detector dark counts ( $\sim 30 \text{ s}^{-1}$ ) and spontaneous decay from the  $P_{3/2}$  state back to  $D_{5/2}$  (with  $5.87\%$  probability [34]).

## VI. CONCLUSIONS

In conclusion, we demonstrated a single-atom to single-photon quantum interface that is programmable to serve for bidirectional quantum-state transfer and generation of atom-photon entanglement, essential operations in quantum networks, especially for a quantum repeater. Entangled ion-photon pairs have been created at close to a  $300 \text{ s}^{-1}$  rate (entangler operation). The reconstructed two-qubit state exhibits  $84.6(2)\%$  fidelity with respect to a maximally entangled state. Using the same ingredients, we realized ion-to-photon quantum-state transfer (sender operation): an arbitrary atomic qubit state is mapped onto the polarization state of the output photon with  $90.2(1.0)\%$  quantum-process fidelity and  $92.4(3)\%$  mean quantum-state fidelity. Application of the same interface for heralded photon-to-atom quantum-state transfer (receiver operation) had been shown earlier [26]. Finally, the converter mode of operation of the interface provides single-photon frequency conversion, with a single atom replacing the conventional nonlinear optical device [35,36]. Our experimental implementation is based on a Raman transition in a single  $^{40}\text{Ca}^+$  ion and is readily adapted to other ions and neutral atoms such as rubidium. Its versatility and simplicity make the interface a valuable tool for quantum repeater and hybrid (see, e.g., [37]) quantum-networking technology.

## ACKNOWLEDGMENTS

We gratefully acknowledge partial support by the BMBF (Germany) through projects QuORP (16BQ1011), QSCALE (Chist-ERA 16BQ1107), and Q.Com-Q (16KIS0127).

- [1] H. J. Kimble, The quantum internet, *Nature* **453**, 1023 (2008).  
 [2] D. Leibfried, B. DeMarco, V. Meyer, D. Lucas, M. Barrett, J. Britton, W. M. Itano, B. Jelenković, C. Langer, T. Rosenband, and D. J. Wineland, Experimental demonstration of a robust, high-fidelity geometric two ion-qubit phase gate, *Nature* **422**, 412 (2003).

- [3] C. Langer, R. Ozeri, J. D. Jost, J. Chiaverini, B. DeMarco, A. Ben-Kish, R. B. Blakestad, J. Britton, D. B. Hume, W. M. Itano, D. Leibfried, R. Reichle, T. Rosenband, T. Schaez, P. O. Schmidt, and D. J. Wineland, Long-Lived Qubit Memory Using Atomic Ions, *Phys. Rev. Lett.* **95**, 060502 (2005).

- [4] J. Benhelm, G. Kirchmair, C. F. Roos, and R. Blatt, Towards fault-tolerant quantum computing with trapped ions, *Nat. Phys.* **4**, 463 (2008).
- [5] G. Weihs, T. Jennewein, C. Simon, H. Weinfurter, and A. Zeilinger, Violation of Bell's Inequality Under Strict Einstein Locality Conditions, *Phys. Rev. Lett.* **81**, 5039 (1998).
- [6] X.-S. Ma, T. Herbst, T. Scheidl, D. Wang, S. Kropatschek, W. Naylor, B. Wittmann, A. Mech, J. Kofler, E. Anisimova, V. Makarov, T. Jennewein, R. Ursin, and A. Zeilinger, Quantum teleportation over 143 kilometres using active feed-forward, *Nature* **489**, 269 (2012).
- [7] M. K. Tey, Z. Chen, S. A. Aljunied, B. Chng, F. Huber, G. Maslennikov, and C. Kurtsiefer, Strong interaction between light and a single trapped atom without the need for a cavity, *Nat. Phys.* **4**, 924 (2008).
- [8] G. Vittorini, D. Hucul, I. V. Inlek, C. Crocker, and C. Monroe, Entanglement of distinguishable quantum memories, *Phys. Rev. A* **90**, 040302(R) (2014).
- [9] R. Maiwald, D. Leibfried, J. Britton, J. C. Bergquist, G. Leuchs, and D. J. Wineland, Stylus ion trap for enhanced access and sensing, *Nat. Phys.* **5**, 551 (2009).
- [10] M. Fischer, M. Bader, R. Maiwald, A. Golla, M. Sondermann, and G. Leuchs, Efficient saturation of an ion in free space, *Appl. Phys. B* **117**, 797 (2014).
- [11] C. J. Hood, M. S. Chapman, T. W. Lynn, and H. J. Kimble, Real-Time Cavity QED with Single Atoms, *Phys. Rev. Lett.* **80**, 4157 (1998).
- [12] M. Hennrich, T. Legero, A. Kuhn, and G. Rempe, Vacuum-Stimulated Raman Scattering Based on Adiabatic Passage in a High-Finesse Optical Cavity, *Phys. Rev. Lett.* **85**, 4872 (2000).
- [13] A. B. Mundt, A. Kreuter, C. Becher, D. Leibfried, J. Eschner, F. Schmidt-Kaler, and R. Blatt, Coupling a Single Atomic Quantum Bit to a High Finesse Optical Cavity, *Phys. Rev. Lett.* **89**, 103001 (2002).
- [14] M. Keller, B. Lange, K. Hayasaka, W. Lange, and H. Walther, Deterministic coupling of single ions to an optical cavity, *Appl. Phys. B* **76**, 125 (2003).
- [15] B. B. Blinov, D. L. Moehring, L.-M. Duan, and C. Monroe, Observation of entanglement between a single trapped atom and a single photon, *Nature* **428**, 153 (2004).
- [16] J. Volz, M. Weber, D. Schlenk, W. Rosenfeld, J. Vrana, K. Saucke, C. Kurtsiefer, and H. Weinfurter, Observation of Entanglement of a Single Photon with a Trapped Atom, *Phys. Rev. Lett.* **96**, 030404 (2006).
- [17] A. D. Boozer, A. Boca, R. Miller, T. E. Northup, and H. J. Kimble, Reversible State Transfer between Light and a Single Trapped Atom, *Phys. Rev. Lett.* **98**, 193601 (2007).
- [18] T. Wilk, S. C. Webster, A. Kuhn, and G. Rempe, Single-atom single-photon quantum interface, *Science* **317**, 488 (2007).
- [19] A. Stute, B. Casabone, B. Brandstätter, K. Friebe, T. E. Northup, and R. Blatt, Quantum-state transfer from an ion to a photon, *Nat. Photon.* **7**, 219 (2013).
- [20] D. L. Moehring, P. Maunz, S. Olmschenk, K. C. Younge, D. N. Matsukevich, L.-M. Duan, and C. Monroe, Entanglement of single-atom quantum bits at a distance, *Nature* **449**, 68 (2007).
- [21] J. Hofmann, M. Krug, N. Ortegel, L. Gérard, M. Weber, W. Rosenfeld, and H. Weinfurter, Heralded entanglement between widely separated atoms, *Science* **337**, 72 (2012).
- [22] S. Olmschenk, D. N. Matsukevich, P. Maunz, D. Hayes, L.-M. Duan, and C. Monroe, Quantum teleportation between distant matter qubits, *Science* **323**, 486 (2009).
- [23] C. Nölleke, A. Neuzner, A. Reiserer, C. Hahn, G. Rempe, and S. Ritter, Efficient Teleportation Between Remote Single-Atom Quantum Memories, *Phys. Rev. Lett.* **110**, 140403 (2013).
- [24] C. Kurz, J. Huwer, M. Schug, P. Müller, and J. Eschner, A high-rate source for single photons in a pure quantum state, *New J. Phys.* **15**, 055005 (2013).
- [25] M. Schug, J. Huwer, C. Kurz, P. Müller, and J. Eschner, Heralded Photonic Interaction between Distant Single Ions, *Phys. Rev. Lett.* **110**, 213603 (2013).
- [26] C. Kurz, M. Schug, P. Eich, J. Huwer, P. Müller, and J. Eschner, Experimental protocol for high-fidelity heralded photon-to-atom quantum state transfer, *Nat. Commun.* **5**, 5527 (2014).
- [27] H.-J. Briegel, W. Dür, J. I. Cirac, and P. Zoller, Quantum Repeaters: The Role of Imperfect Local Operations in Quantum Communication, *Phys. Rev. Lett.* **81**, 5932 (1998).
- [28] M. Schug, C. Kurz, P. Eich, J. Huwer, P. Müller, and J. Eschner, Quantum interference in the absorption and emission of single photons by a single ion, *Phys. Rev. A* **90**, 023829 (2014).
- [29] F. Rohde, M. Almendros, C. Schuck, J. Huwer, M. Hennrich, and J. Eschner, A diode laser stabilization scheme for  $^{40}\text{Ca}^+$  single-ion spectroscopy, *J. Phys. B* **43**, 115401 (2010).
- [30] S. Gerber, D. Rotter, M. Hennrich, R. Blatt, F. Rohde, C. Schuck, M. Almendros, R. Gehr, F. Dubin, and J. Eschner, Quantum interference from remotely trapped ions, *New J. Phys.* **11**, 013032 (2009).
- [31] E. Togan, Y. Chu, A. S. Trifonov, L. Jiang, J. Maze, L. Childress, M. V. G. Dutt, A. S. Sorensen, P. R. Hemmer, A. S. Zibrov, and M. D. Lukin, Quantum entanglement between an optical photon and a solid-state spin qubit, *Nature* **466**, 730 (2010).
- [32] D. F. V. James, P. G. Kwiat, W. J. Munro, and A. G. White, Measurement of qubits, *Phys. Rev. A* **64**, 052312 (2001).
- [33] I. L. Chuang and M. A. Nielsen, Prescription for experimental determination of the dynamics of a quantum black box, *J. Mod. Opt.* **44**, 2455 (1997).
- [34] R. Gerritsma, G. Kirchmair, F. Zähringer, J. Benhelm, R. Blatt, and C. F. Roos, Precision measurement of the branching fractions of the  $4p^2 P_{3/2}$  decay of Ca II, *Eur. Phys. J. D* **50**, 13 (2008).
- [35] R. Ikuta, Y. Kusaka, T. Kitano, H. Kato, T. Yamamoto, M. Koashi, and N. Imoto, Wide-band quantum interface for visible-to-telecommunication wavelength conversion, *Nat. Commun.* **2**, 537 (2011).
- [36] S. Zaske, A. Lenhard, C. A. Keßler, J. Kettler, C. Hepp, C. Arend, R. Albrecht, W.-M. Schulz, M. Jetter, P. Michler, and C. Becher, Visible-to-Telecom Quantum Frequency Conversion of Light from a Single Quantum Emitter, *Phys. Rev. Lett.* **109**, 147404 (2012).
- [37] H. M. Meyer, R. Stockill, M. Steiner, C. Le Gall, C. Matthiesen, E. Clarke, A. Ludwig, J. Reichel, M. Atatüre, and M. Köhl, Direct Photonic Coupling of a Semiconductor Quantum Dot and a Trapped Ion, *Phys. Rev. Lett.* **114**, 123001 (2015).